UNIVERSITY OF TECHNOLOGY SYDNEY

PAM Review

Subject 68412
www.uts.edu.au

Solar Power Concentrators for Space Applications

Joshua Pritchard [1*], Kiri Simon [2], Cameron Dowd [3] and Eashwar Joshi [4]
Faculty of Science, University of Technology Sydney, P.O Box 123, Australia

[1] E-Mail: Joshua.A.Pritchard@student.uts.edu.au
[2] E-Mail: Kiri.C.Simon@student.uts.edu.au
[3] E-Mail: Cameron.Dowd@student.uts.edu.au
[4] E-Mail: Eashwar.Joshi-1@student.uts.edu.au

* Author to whom correspondence should be addressed.

DOI: http://dx.doi.org/10.5130/pamr.v3i0.1413

Abstract: Space based solar power is an attractive solution to growing energy needs, overcoming the operational downtime and atmospheric losses inherent to terrestrial solar technologies. Ideal solar satellites include concentrator systems in order to produce a high specific power output, keeping mass low for economic launch. A meta analysis of photovoltaic concentrator research is presented to determine viability in space applications, considering contributions to cell heating, subcell current matching and efficiency of the InGaP/GaAs/Ge multi-junction cell. We find that the CaF_2 Fresnel lens is an optimal choice with an efficiency increase of 4.9% at 17 suns. The large range of concentration ratio, low mass, compact design and minimal effect on spectral irradiance allow a wide space for optimisation in temperature control, whilst the current matching conditions under concentration can be regulated by appropriate tunnel junction width and bandgap.

Keywords: InGaP/GaAs/Ge, Solar, Cell, Photovoltaic, Multi-Junction, Satellite, Concentrator

---

1. Introduction

1.1 Solar Power Satellites

Solar technology within Earth's atmosphere provides a number of natural disadvantages to the levels of efficiency that would see solar power be a leading source of power in world. The atmosphere provides a filter that preserves humans from the deadlier aspects of the Sun's radiation, but also removes a lot of the higher energy spectrum rays through reflection, scattering and absorption, especially at the upper and lower latitudes. So, too, do seasonal changes create a large fluctuation in available light flux over the course of the seasons. When added to the crowded natures of our cities, with their overshadowing structures, constant energy demands, and inadequate energy storage capability for winter and night-time energy demand, solar power faces many very real challenges that drive the development of ever more efficient photovoltaics cells, and associated energy storage systems.

However, solar irradiance levels just beyond Earth's atmosphere provide access to a far greater spectrum of photon energies for solar cells, which can be purpose-built to take advantage of the unfiltered irradiance. The idea of space based solar power (SBSP) has been around since the late 1960's when Peter Glaser proposed the concept of a solar power satellite (SPS). [1] Such systems would be placed into either an inclined orbit about the Earth or at a Lagrange point in the Earth-Sun system.

Placing solar panels in Earth orbit or positioned at a Lagrange point, would give access to constant sunlight, greater concentrations of higher-energy photons, and require minimal energy usage in the case of the Lagrange point; with little need to provide extra module thrust, unlike satellites in Earth-orbit that must constantly adjust their orbital path to fight the effects of atmospheric drag. Within space new challenges arise for efficient heat-sinking, radiation damage prevention and temperature control, and design constraints must be placed upon any system in orbit, as overall mass and dimensions are limited by the enormous financial and energy costs of launch. The power gains rival the potential of terrestrial counterparts, and outstrip them for powering space-based projects. [2-3]

Satellite heating is dependent on a number of factors; primarily direct solar irradiance, reflection and thermal emission from the Earth and internal heating due to power dissipation. The thermal emission of other bodies such as the moon and planets is negligible. The Sun's spectral irradiance is well approximated by a 6000K black body following Planck's radiation law. The total intensity of solar radiation is then found by integrating across all wavelengths to give the Stefan-Boltzmann law. [4]

$$\int_0^\infty \boldsymbol{F(\lambda)\, d\lambda} = \frac{\boldsymbol{2\pi^5 k^4}}{\boldsymbol{15 h^3 c^2}} \boldsymbol{T^4} = \boldsymbol{\sigma T^4} \tag{1}$$

The Sun is closer to 5777K, and thus radiates 63.2 MW per square meter of solar surface. That intensity is less at the orbital distance of the Earth, accounting for a factor of decrease in flux of 4.62 x 10^4 leaves us with a solar constant $\boldsymbol{E_S}$ of 1366 Wm^{-2}. As the Earth is in thermal equilibrium with this irradiance it must emit an equal quantity, rearranging this equality we can approximate the effective temperature of Earth:

$$\boldsymbol{4\pi R_{\oplus}^2 \sigma T_{\oplus}^4 = \sigma T_{\odot}^4 \frac{R_{\odot}^2}{a_0^2} \pi R_{\oplus}^2}$$

$$\boldsymbol{\rightarrow T_{\oplus} = T_{\odot} \sqrt{\frac{R_{\odot}}{2a_0}} \approx 279K} \quad (2)$$

where $R_{\oplus}$, $R_{\odot}$, $T_{\oplus}$ and $T_{\odot}$ are the radii and effective temperatures of the Earth and Sun respectively, and $\boldsymbol{a_0}$ is the distance from the Earth to the Sun.

Whilst the solar irradiance is incident upon the photovoltaic cell where a portion of the energy is converted to useful work, the radiation from Earth is either reflected or absorbed by the rest of the satellite contributing to heating. The total irradiance absorbed by the satellite is then:

$$\boldsymbol{E_{ABS} = T_{AR} E_S (1 - \eta) + A_{BULK} (\alpha E_S + \sigma T_{\oplus}^4)} \quad (3)$$

where $\boldsymbol{T_{AR}}$ is the transmittance of the photovoltaic cell's anti-reflective coating, $\boldsymbol{A_{BULK}}$ is the absorbance of the bulk cell, $\boldsymbol{\eta}$ is the cell efficiency and $\boldsymbol{\alpha}$ is the Earth's albedo.

1.2 Photovoltaic Cells

1.2.1 Efficiency Limits

The photovoltaic cell can be approximated as a heat engine, collecting energy from a hot reservoir of blackbody radiation and cooling it through the photovoltaic effect. [5] Incident photons lose kinetic energy by giving valence electrons in the cell potential energy as they jump to the conduction band. The bandgap energy required to make this jump is then available to be collected as work in an external circuit by collecting the electron as it is accelerated by a potential.

The heat engine approximation determines an upper limit for the efficiency of such a system, and applying the principle of detailed balance leads to the Carnot efficiency:

$$\boldsymbol{\eta_{CARNOT} = \frac{W}{E_S} = 1 - \frac{Q}{E_S} = 1 - \frac{T_A}{T_S}} \quad (4)$$

where $\boldsymbol{T_A}$ and $\boldsymbol{T_S}$ are the ambient and solar temperatures respectively.

In contrast to conductive transfer, where a temperature gradient causes entropy to increase towards the cold reservoir, entropy is conserved in radiative energy transfer and can be calculated for a black body from the second law of thermodynamics: [6]

$$\boldsymbol{S_S = \frac{4}{3}\frac{E_S}{T_S}} \tag{5}$$

Once accounting for this $\frac{4}{3}$ factor, the Carnot efficiency has new terms introduced that result from entropy fluxes from the blackbody radiation reservoir and cell. The Landsberg efficiency is a thermodynamic limit upon how much work can be extracted from this blackbody radiation. [6]

$$\boldsymbol{\eta_{LANDSBERG} = 1 - \frac{4}{3}\frac{T_A}{T_S} + \left(\frac{T_C}{T_S}\right)^4 \left(\frac{4}{3}\frac{T_A}{T_C} - 1\right)} \tag{6}$$

where $\boldsymbol{T_C}$ is the temperature of the cell.

Taking $\boldsymbol{T_A = T_C = 300K}$ and $\boldsymbol{T_S = 6000K}$, the ultimate thermodynamic capability of a photovoltaic cell is 93.3%. There are countless engineering challenges and inefficiencies that bring this number to less than half of the theoretical maximum, and it is in those inefficiencies that improvements can be made.

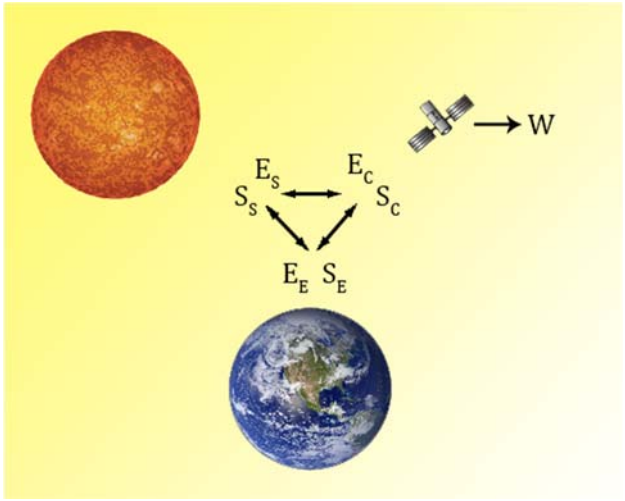

Figure 1. Overview of energy and entropy flux in a SPS system. E_S and S_S represent the direct solar irradiance, E_E and S_E are comprised of the Earth's black body radiation and reflected solar irradiance, E_C and S_C represent inefficiencies in the solar cell, blackbody radiation and reflected light. W is the useful power extracted from the system.

1.2.2 Multi-Junction Cells

When a valence electron absorbs an incident photon, energy is transferred to the electron allowing it to jump to the conduction band, leaving a hole in the valence band. The charge carriers are then free to move and can be accelerated by a voltage. In a photovoltaic cell that voltage is supplied by an electric field created by the depletion region in the p-n junction. Ideally excess photon energy would contribute to the effective voltage, but these "hot" carriers lose kinetic energy to phonon interactions with the crystal lattice, quickly thermalising to the bottom of the conduction band. There is then a trade-off between low bandgap materials which harness more low energy photons but lose a great deal of energy in the blue end of the spectrum, and wide bandgap materials which more efficiently capture high energy photons whilst missing the red light completely.

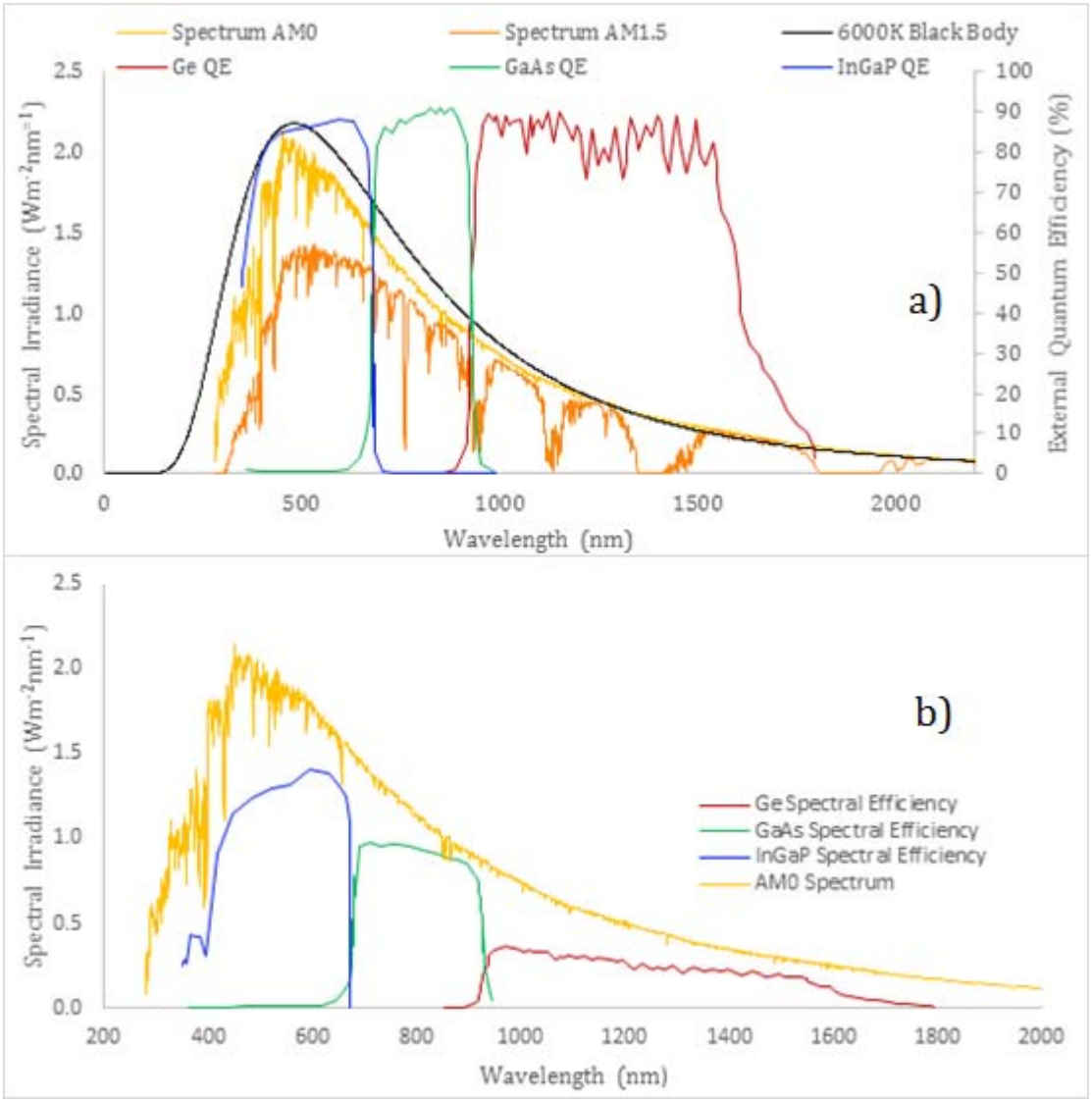

Figure 2. a) Spectral response of a C4MJ InGaP/GaAs/Ge multijunction cell against atmospheric mass zero and 1.5 (AM0) and (AM1.5) and blackbody spectra. b) Quantum efficiency curves are convolved with AM0 spectrum and normalized to each cell bandgap. The area between

spectral efficiency curves and the spectrum is lost to imperfect quantum efficiency or thermalisation as the photon energy exceeds the bandgap. [7-8]

One solution to this inefficiency is to stack several subcells on top of one another, connected in series as a multi-junction cell (Fig 2.). Subcells are stacked from wide bandgap at the top to narrow at the bottom, such that each cell will collect photons above its bandgap and transmit lower energy light to the next subcell. An infinite number of cells with incremental differences in bandgap would then theoretically collect light with perfect efficiency, losing no energy to thermalisation. [9] In reality several factors prevent such a perfect cell; non-uniform quantum efficiency, scarcity of materials with suitable bandgap and lattice matching structure among them.

Multi-junction cells are currently available with up to 5 junctions [10], with a popular 3-junction configuration consisting of a 1.86 eV *Indium Gallium Phosphide* (InGaP) top cell, 1.42 eV *Gallium Arsenide* (GaAs) middle cell and 0.66 eV *Germanium* (Ge) bottom cell.

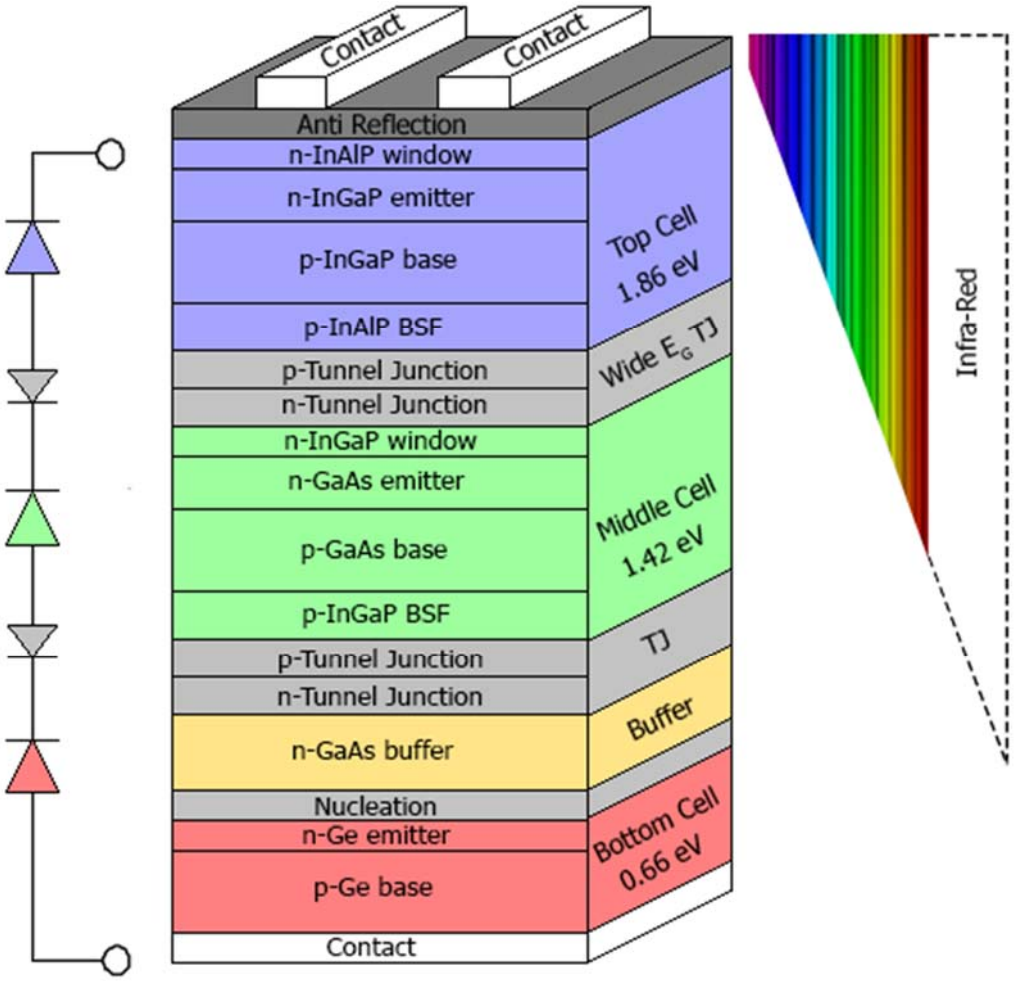

Figure 3. Multi-junction cell design and solar spectrum penetration depth depicted. Circuit diagram displays each subcell in forward bias and tunnel junctions in reverse bias.

1.2.3 J_{SC}, V_{OC} and Fill Factor

A photovoltaic cell's power generation is the product of its photo-generated current (I_L) and voltage corresponding to the cell bandgap. Charge carriers that are separated across this potential are collected by energy-selective contacts to be used in an external circuit. Extracting maximum power from the cell is then a matter of attaining the maximum product of these two quantities. However, as previously explored, increased voltage with a wide bandgap comes at the cost of excluded low energy photons, and therefore less current.

Short-circuit current density (J_{SC}) is the photo-generated current density (J_L) produced by a cell with no series resistance. J_{SC} is dependent upon the flux and spectrum of incident photons and carrier generation rate, which itself depends upon the cell's absorption coefficient (α) and thickness. Cells will realistically have some series resistance (R_S) contributed to by the semiconductor and contacts. [10] When under no illumination, photovoltaic cells still produce a current density, but in opposition to J_L. Diffusion of minority charge carriers into the depletion region results in a dark saturation current density J_0:

$$\boldsymbol{J_0 = e\left(\sqrt{\frac{D_P}{\tau_P}}\frac{n_i^2}{N_D} + \sqrt{\frac{D_n}{\tau_n}}\frac{n_i^2}{N_A}\right)} \tag{7}$$

where $D_{p,n}$ and $\tau_{p,n}$ are the diffusion coefficients and carrier lifetimes of holes and electrons respectively, n_i is the intrinsic carrier concentration and $N_{D,A}$ are the donor and acceptor concentrations at the n and p sides respectively. [11]

The maximum voltage available from a photovoltaic cell is equivalent to the bias at which J_L is equal to J_0 and no current flows. This is the open-circuit voltage (V_{OC}), and will be limited by the potential induced by the bandgap. V_{OC} is lower than the bandgap due to recombination processes in which conduction band electrons fall back to the valence band. The energy is either radiated away as a photon (radiative recombination) or excites another conduction band electron and is lost to thermalisation (Auger recombination). [11] More specifically the V_{OC} arises due to a chemical potential difference between electron and hole populations in the conduction and valence band respectively:

$$\boldsymbol{V_{OC} = \frac{kT}{q}\ln\left(\frac{J_L}{J_0} + 1\right) = \frac{kT}{q}\ln\left[\frac{(N_A + \Delta n)\Delta n}{n_i^2}\right]} \tag{8}$$

where Δn is the excess carrier concentration. [11]

Taking the product of J_{SC} and V_{OC} produces the ideal maximum power that can be drawn from a given cell area, represented by the area under the J-V curve. As these quantities are dependent on one another the realistic maximum power drawn from the system is some fraction of the I_{SC}-V_{OC} product. Fill factor is then defined as the ratio of realistic to ideal power draw:

$$\boldsymbol{FF = \frac{J_{MP}V_{MP}}{J_{SC}V_{OC}}} \tag{9}$$

where I_{MP} and V_{MP} are the current and voltage that produce the maximum power. Fill factor is limited by any reduction in V_{OC} or J_{SC}, as well as parasitic resistance that affects the J-V relationship.

1.2.4 Current Matching

Optimum efficiency in a multi-junction cell is further limited by the subcell with the lowest current density, as the subcells are wired in series (Fig. 2). Subcells should therefore be closely matched in current density to minimize power loss to heat. The current density produced by each subcell will depend upon the incident spectrum, bandgap, quantum efficiency, thickness and absorption coefficient of the cell. Bandgap determines which portion of the incident spectrum the subcell is sensitive to, whilst the quantum efficiency, thickness and absorption coefficient determine the probability of a photon interacting with an electron to produce a charge carrier.

2. Methods

Solar concentrator designs are well researched and varied in their approach to terrestrial concentrated photovoltaic applications, though many concentrator designs include benefits such as solar-tracking, wide acceptance angles and diffuse light gathering which have limited or no use in space applications. Other design choices affecting the dimensions and mass may have limited impact on land, but render the system useless for SBSP due to restrictive launch costs and orbital environment limitations; in space there is higher spectral irradiance without atmospheric absorption, constant irradiation without dusk/dawn/night inefficiency and high temperature due to no convective or conductive heat dissipation. This motivated a meta-study into the viability of concentrator systems in a space environment, distinguishing landlocked designs from those which make use of the unique environment of space.

Literature was searched through Scopus, Web of Science and Google Scholar to include works not included in the databases. The following keywords were used: ‘solar power satellite’, ‘multi junction’, ‘photovoltaic’, ‘InGaP/GaAs/Ge’, ‘Indium Gallium Phosphide’, ‘Gallium Arsenide’, ‘Germanium’, ‘bandgap’, ‘concentrator’, ‘Fresnel’, ‘temperature dependence’, ‘efficiency’, ‘thermodynamic’ in various combinations. We analysed a wide range of papers before identifying some of the primary parameters that regulate photovoltaic efficiency, namely temperature, subcell thickness, tunnel junction composition, and the spectral characteristics of incident light. They dictate V_{OC}, $J_{SC,}$ fill factor and subcell current matching, affecting overall power output and efficiency. With these variables in mind results were further narrowed to publications within the last 20 years which focused on concentrator designs used in conjunction with InGaP/GaAs/Ge multijunction cells.

Meta-analysis was conducted on 36 papers meeting our criteria, highlighting 7 prominent concentrator designs; the Fresnel lens, micro-lens array, parabolic trough, hyperboloid, quantum dot concentrator, compound parabolic concentrator (CPC) and dielectric totally internal reflecting

concentrator (DTIRC). The hyperboloid, parabolic trough and CPC designs were omitted from final results as they feature geometries too debilitating for SBSP. Hyperbolic and parabolic concentrators are well suited to gathering diffuse light from extreme incidence angles but cannot reach large concentration ratios for direct irradiance without excessive length and mass.

3. Results and Discussion

3.1 Temperature Dependence

Regularly spaced atoms in the crystal lattice give rise to a periodic potential which the electrons are subject to. Increases in lattice temperature cause inter-atomic bonds to oscillate with more energy and atomic spacing increases. As the atomic spacing increases the average potential decreases, resulting in a reduction in bandgap energy. A second temperature dependent mechanism is the vibration of atoms. As temperature increases the phonon energy also increases, leading to electrons in the valence band requiring less energy to make the jump to the conduction band when assisted by a phonon interaction. Band gap energy is therefore a function of lattice temperature, following the Varshni relationship:

$$E_g = E_0 - \frac{\alpha T^2}{T + \beta} \tag{10}$$

where E_0 is the bandgap at 0K and α and β are fitting constants. [13]

Table 1. Thermal characteristics of junction materials. [14]

Material	***E_0 (eV)***	***α (eV/K)***	***β (K)***
InGaP	1.915	3.10×10^{-4}	248
GaAs	1.5216	5.41×10^{-4}	204
Ge	0.742	4.81×10^{-4}	235

In AM0 conditions, temperatures of solar cells tend to be higher, and efficiencies slightly lower, than under terrestrial conditions due to the increased spectral irradiance. Reduction in bandgap at high temperature leads to lower-energy incident photons bridging the bandgap, higher recombination rates and higher current carrier numbers with subsequent lower open-circuit voltage. High temperatures also degrade cell structures over time by causing irreversible dopant diffusion. [15-17] Currently, maximum average efficiency attained for this style of triple-junction cell is 38% to 39% at 298 K and AM0. [18]

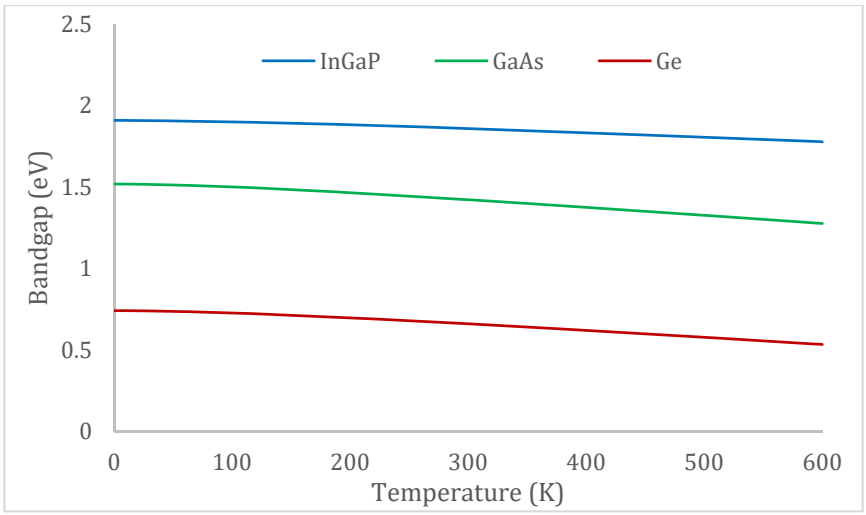

Figure 4. Calculated semiconductor bandgaps as a function of cell temperature.

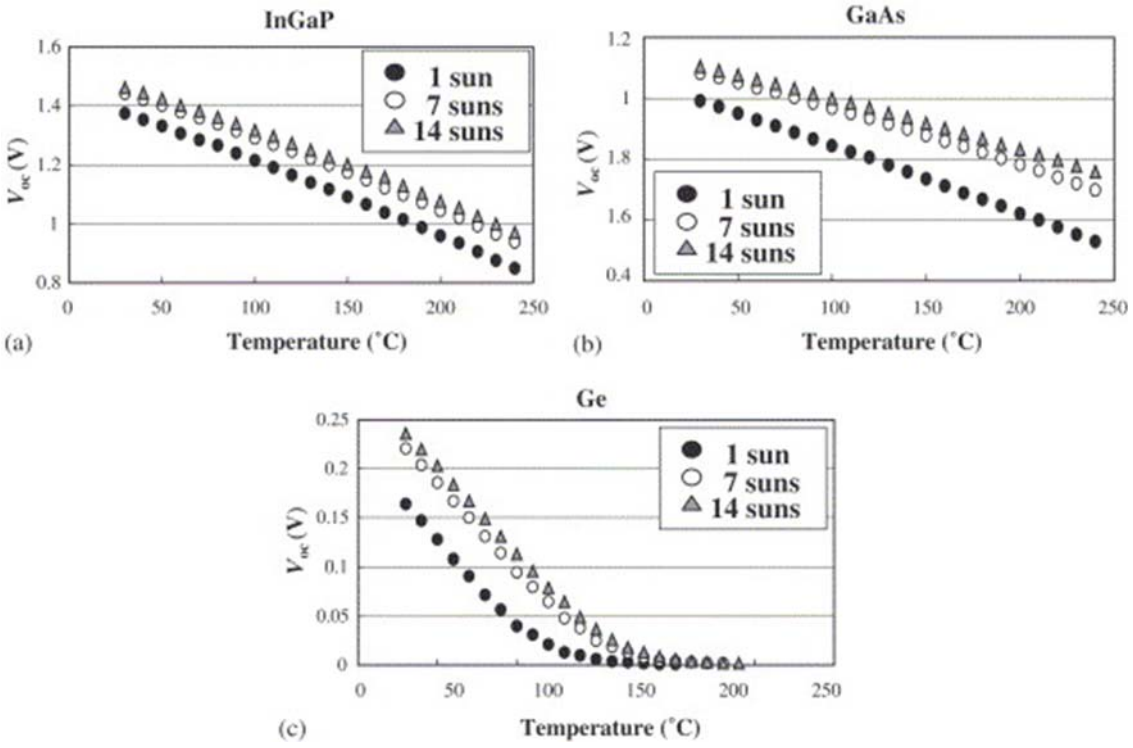

Figure 5. Drop in V_{OC} of a) InGaP, b) GaAs and c) Ge subcells as a function of temperature are several concentration ratios. [16]

3.2 Tunnel junctions

Multi-junction cells suffer voltage losses when neighbouring subcells form a parasitic p-n junction that opposes the n-p junctions producing photocurrent (Fig 2.). Tunnel junctions are heavily-doped, thin p-n junctions situated between the offending sub-cells as a low resistance, optically transparent connection. Electrons are able to quantum tunnel through the low voltage region in the thin layer to vacant energy states on the other side. The tunnelling current experiences extremely low resistance and

minimal voltage drop, allowing the photogenerated power of upper subcells to be effectively transported through the lower layers. [19-21]

Different portions of the incident spectrum on the multijunction cell are captured by the three sub-cells. The tunnel junction between the InGaP and GaAs layers can absorb a portion of the light transmitted by the top layer before it can reach the layer beneath. Photogenerated current in these layers is in opposition to the rest of the cell and considered parasitic. Wide bandgap materials are then desirable to make the tunnel junction optically transparent to the low energy light; however, they also increase the chemical potential in the p-n junction, presenting a large potential barrier to tunnelling electrons and therefore less current. [22] Furthermore, the tunnel junction in the multijunction cell needs to be highly doped (in excess of 10^{19} cm^{-3}), but it is difficult to dope materials with high bandgaps as the dopant level is a function of peak tunnelling current. [10] There therefore exists a trade-space for optimizing the tunnelling current and photon transmission in tunnel junctions. [23-24]

In concentrator multijunction cells, the high photon intensity increases the current density of the overall cell (Fig. 6). Consequently, this requires the peak tunnelling current density to be significantly higher than the cell's photocurrent density in order to avoid the tunnel junction photolimiting the cell under high concentration conditions. If the photocurrent generated by the multijunction cell is less than the peak tunnelling current, the tunnel junction has minimal ohmic resistance and acts like a standard electrical contact between neighbouring subcells. Once this peak tunnelling current has been exceeded however, there appears a steep drop in tunnelling current density which limits the overall photocurrent of the cell. [25-28]

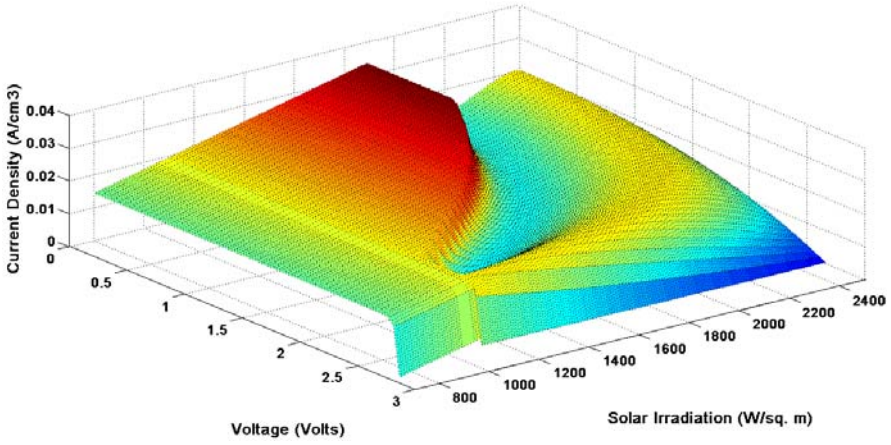

Figure 6. Current density, voltage and solar irradiance characteristic of a *InGaP, GaAs, Ge* multijunction cell. [28]

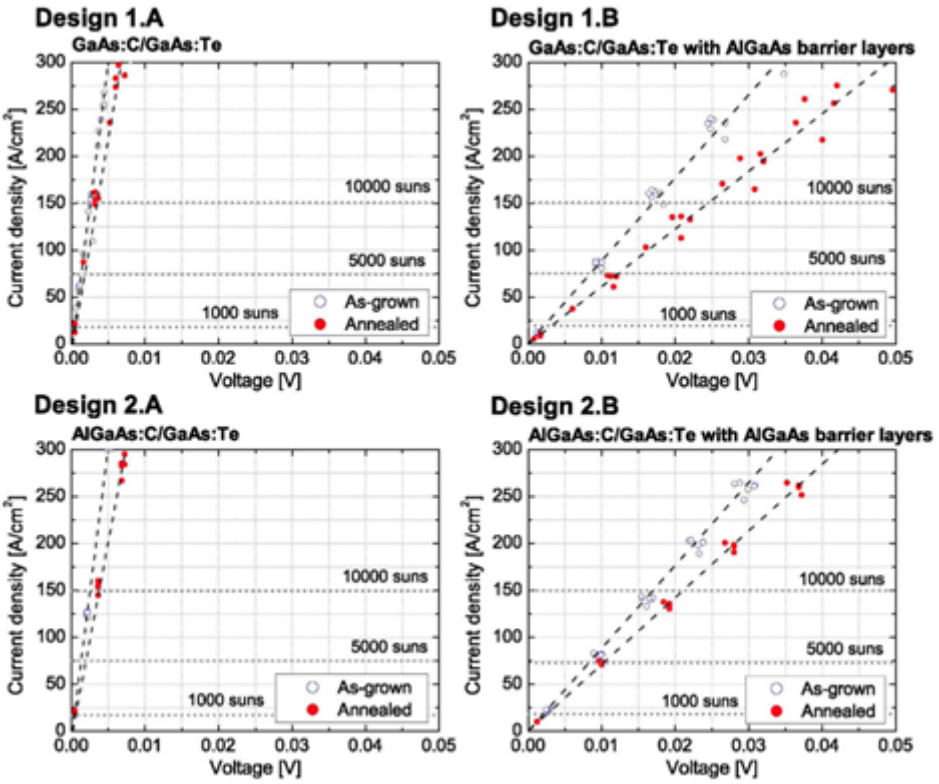

Figure 7. J-V characteristics of four AlGaAs/GaAs tunnel junction designs. [51]

3.3 Incident Concentration

Changing incident intensity affects many solar cell parameters, including I_{SC}, V_{OC}, FF, η, and the effect of resistances. [17,29] As a higher photon flux irradiates the cell the average potential between carrier populations increases. V_{OC} scales logarithmically with the J_L/J_0 ratio (Eq. 8), resulting in a slow increase in efficiency with increased photocurrent density.

3.3.1 Fresnel Lens

The Fresnel lens is a compact, low focal ratio design of solar concentrator that has an equivalent concentrating power to a bulkier plano-convex lens of similar aperture. Lens material can be removed by dividing the conventional lens into many smaller discrete lens elements, resulting in a much thinner profile.

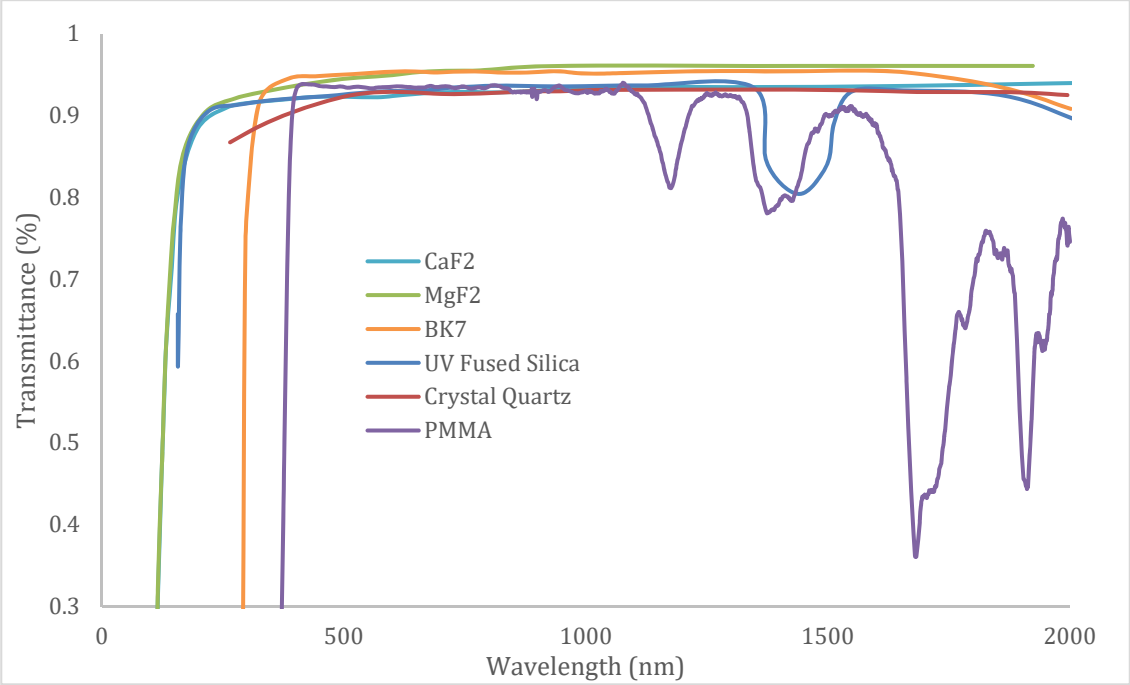

Figure 5. Optical transmittance of various Fresnel lens materials. [30-31]

Lens material has a dramatic effect on efficiency, as absorption bands in different materials alter the incident spectrum. If absorption bands occur within a particular subcell's sensitive range, J_{SC} is reduced harming current matching conditions. Absorption bands may also be outside the useful spectral range, in which case cell performance is relatively unaffected. Although PMMA lenses show absorption bands at 1175 nm, 1395 nm, 1690 nm and 1900 nm (Fig. 5), flux losses are minimal as only the relatively shallow 1175 nm and 1395 nm peaks are within the sensitive range of Germanium.

Optimal choice of lens material is also based on thermal expansion and heat capacity factors, as a lens should be robust to the temperature fluctuations inherent to an object in orbit. Low density materials are crucial in SBSP applications, increasing the specific power output to more quickly offset the energy costs of putting the material into orbit.

Table 2. Lens material properties. [30-31]

Material	***Abbe Number***	***n (λ)$_{400\text{-}2000\ nm}$***	***α (10^{-6} K^{-1})***	***Specific Heat Capacity ($Jg^{-1}K^{-1}$)***	***Density (gcm^{-3})***
CaF_2	94.96	1.44-1.50	18.85	0.85	3.18
MgF_2	106.18	n_O: 1.38-1.43 n_E: 1.40-1.44	13.7 || to c axis 8.48 ⊥ to c axis	1.024	3.177
BK7	64.17	1.53-1.55	7.1	0.858	81.5
UV Fused Silica	67.8	1.48-1.60	0.52	0.75	2.202
Crystal Quartz	69.87	n_O: 1.56-166 n_E: 1.57-1.67	7.1 || to c axis 13.2 ⊥ to c axis	0.74	2.649
PMMA	58.00	1.48-1.51	75	1.46	1.17

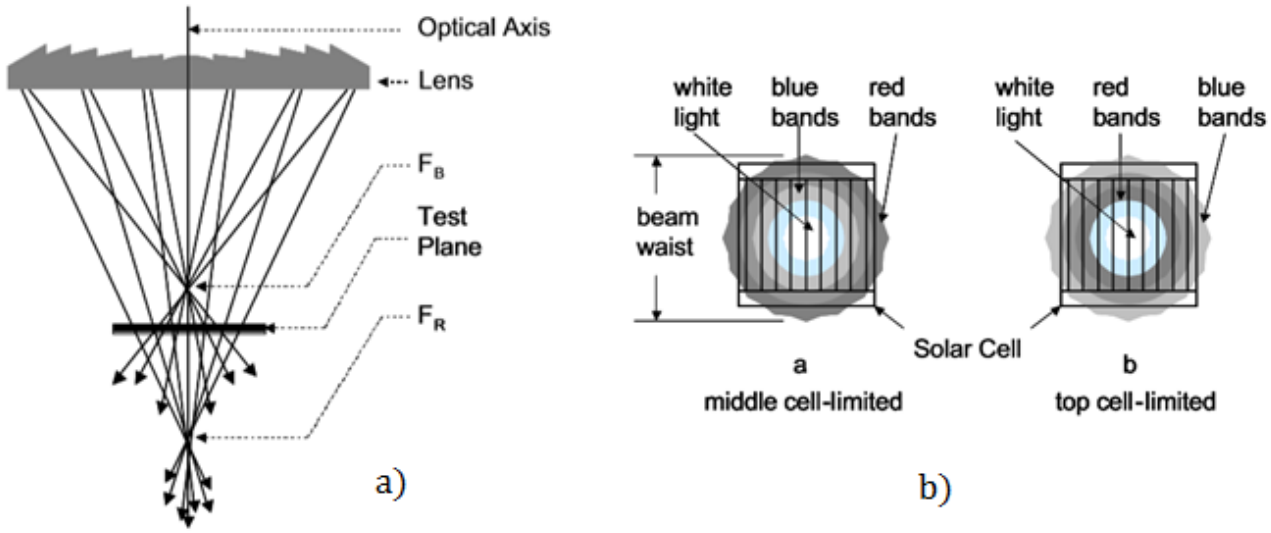

Figure 6. a) Axial chromatic aberration smears the focal point of each wavelength across a range. **b)** Cells can be starved of illumination if lens-cell distance results in uneven spectral focus. [32]

Optimal lens materials feature low measures of dispersion to avoid chromatic aberration, as encoded in the Abbe number:

$$\boldsymbol{V_D = \frac{n_D - 1}{n_F - n_C}} \tag{11}$$

where n_D, n_F and n_C are the wavelengths of the D-, F- and C- Fraunhofer spectral lines at 589.3nm, 486.1 nm and 656.3 nm respectively, and higher V_D corresponds to low dispersion.

Distortion from lens degradation is also a cause of chromatic aberration as well as other optical defects. Thin lenses are desirable to reduce absorptive losses; though rigid structures necessitate some appreciable thickness. Stretched, flexible Fresnel lenses have been proposed for space based concentrator systems, featuring deployable supports that pack into a low-volume stowing configuration. [33]

Excessive axial chromatic aberration can affect cell performance by changing the relative spectral irradiance on each subcell. If positioned too close to the lens blue light will be focused within the cell area, but the red light will be out of focus and the edges of the beam waist will not be collected (Fig. 6b). Conversely if the cell is too far from the lens, red light will be properly focused but blue light will be dispersed missing the cell.

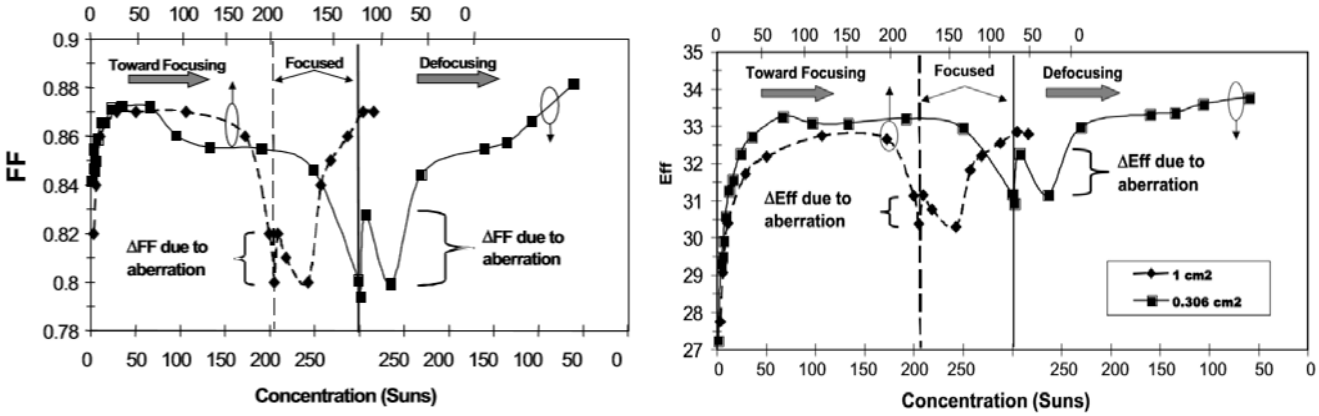

Figure 7. Fill factor and efficiency as a function of concentration due to cell placement. The upper axis represents the solid curve and the lower axis the dashed curve. [33]

Both aberration and lens absorption result in a change in the irradiance on each subcell, with the bottom cell being starved in the former and the top cell in the latter. V_{OC} will be reduced due to a reduction in intensity but the main loss is due to current density mismatch between subcells, the starved cell bottlenecking any excess current density produced by the others. These effects have an impact on the fill factor (ΔFF) and efficiency (ΔEff) of the cell (Fig. 7). Whilst terrestrial systems require mechanical tracking of the Sun to maintain uniform axial aberration, SBSP systems can optimize cell-lens distance for efficient current matching conditions and remain oriented towards the Sun at all times.

3.3.2 Micro Lens Array

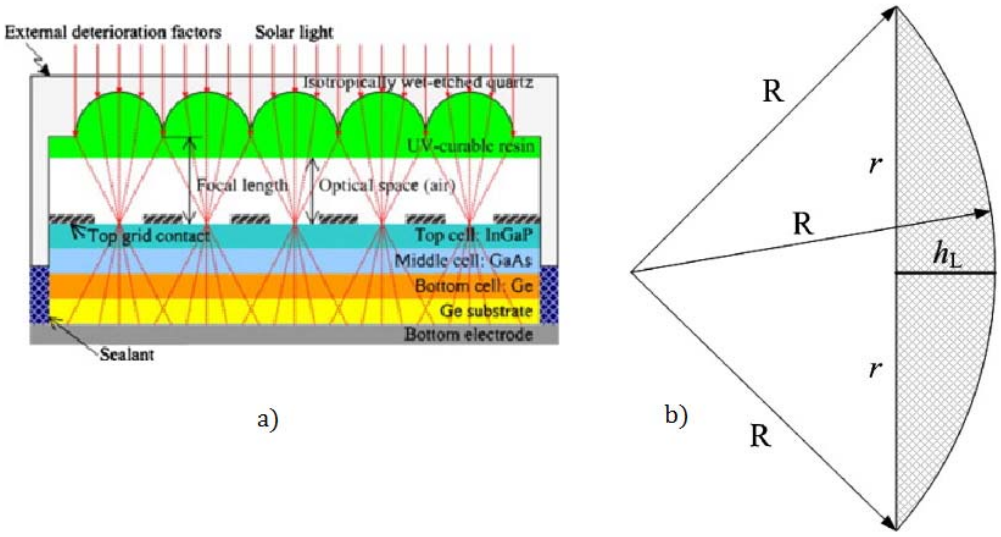

Figure 8. a) An imaging microlens array concentrating sunlight onto an InGaP/GaAs/Ge solar cell. b) Geometry of micro lens curvature. [34]

The micro lens array (MLA) is a concentrator system comprising an array of plano-convex lenses that focus incident light onto the top cell. Maximum flux is transferred to the cell by avoiding the front surface contacts altogether. Lenses are formed from a layer of wet-etched quartz filled in with a cured polymer, and have radius of curvature and focal length:

$$\boldsymbol{R = \frac{(K+1)h_L}{2} + \frac{r^2}{2h_L}} \tag{12}$$

$$\boldsymbol{f = -\frac{R}{n_1 - n_2}} \tag{13}$$

where K is the conic constant (0 in a spherical lens), r is the radius of each microlens, h_L is the etch depth and $n_{1,2}$ are the refractive indices of quartz and the polymer respectively. The quartz encapsulation doubles as a barrier to environmental degradation.

This concentrator system does not have a high concentration ratio, only slightly increasing the intensity received by reducing reflection losses from front surface contacts. Advantages are the longer path length through the cell layers (Fig. 8), leading to increased carrier generation for the same subcell thickness and therefore higher current density (Fig. 9).

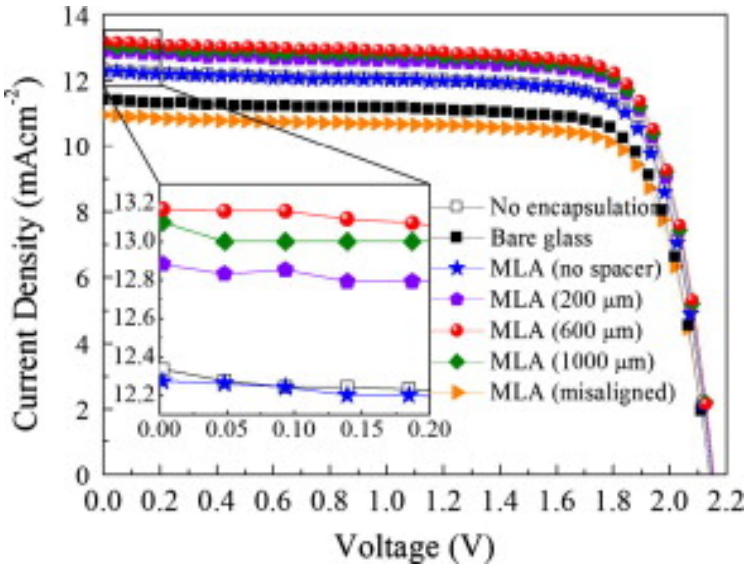

Figure 9. J-V characteristics of an InGaP/GaAs/Ge cell under a range of MLA configurations. [34]

The addition of Fresnel lenses in place of the plano-convex could further improve the benefits of MLA systems by reducing the array thickness, and the aforementioned lens material parameters are equally important to the efficiency of this system.

3.3.3 Quantum Dot Concentrators

Quantum dots (QD) are under experimentation in use as frequency tuning luminescent solar concentrators (LSC). [38] QD diameters are on the same scale as their excitons' Bohr radius, confining

the electron-hole pair in all 3 dimensions, which separates their energy bands into discrete levels. They are deposited onto one or more of the solar cell's layers, or throughout a flat pane to which a photovoltaic cell is affixed (Fig. 10a). Incident sunlight is absorbed and re-emitted by the QDs at a size dependent frequency (Fig. 10b), with mirrors on the internal surfaces of the pane reflecting the emissions though to the photovoltaic adjunct.

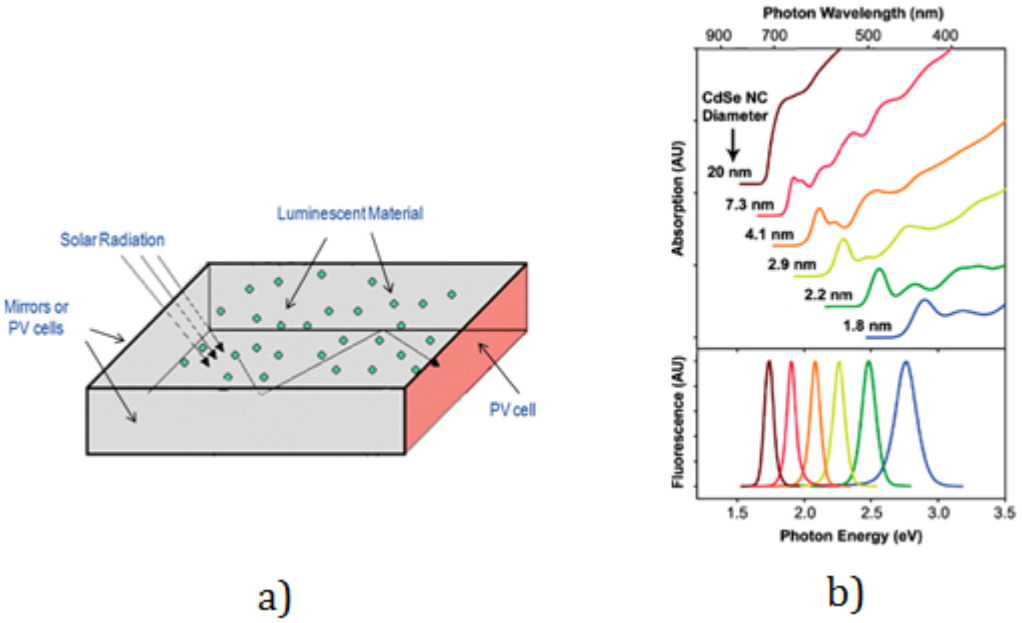

Figure 10. a) Quantum dot concentrator design. b) Stokes shift in absorption/emission spectra. Larger Stokes shift is desirable for quantum dot concentrators to reduce absorption/emission spectra overlap, decreasing the risk of photon loss through non-radiative recombination. [35-36]

Concentration ratio of quantum solar concentrators as a ratio of the incoming flux on the collection surface to outgoing flux through to the photovoltaic cell. The optical efficiency is determined by absorption and collection efficiencies, where absorption efficiency represents the fraction of incident photons that are absorbed by the quantum dots, and collection efficiency is the fraction of these absorbed photons that reach the photovoltaic cell.

Concentrators operate at an efficiency regulated by the product of collection efficiency with absorption efficiency, and efficiency per absorbed photon. The photon absorption/emission spectra difference is known as the Stokes shift, in which a large Stokes shift is desirable, indicating a smaller overlap in absorption and emission bands, decreasing the risk of photon loss through non-radiative recombination.

One of the notable features of quantum dots is that a dot can produce multiple electron-hole pairs from the incidence of one photon, thereby utilizing the portion of the incident light's energy that exceeds the bandgap and re-emitting at lower energies which are often more compatible with the multijunction cell. This increases photocurrent in the solar cell thereby improving the efficiency, as well as decreasing heat by-product. This is known as photon downshifting and makes quantum dots thermally more stable

than other concentrator devices. Similarly, upshifting quantum dots can absorb multiple lower energy photons in the infra-red range and re-emit them as higher energy photons.

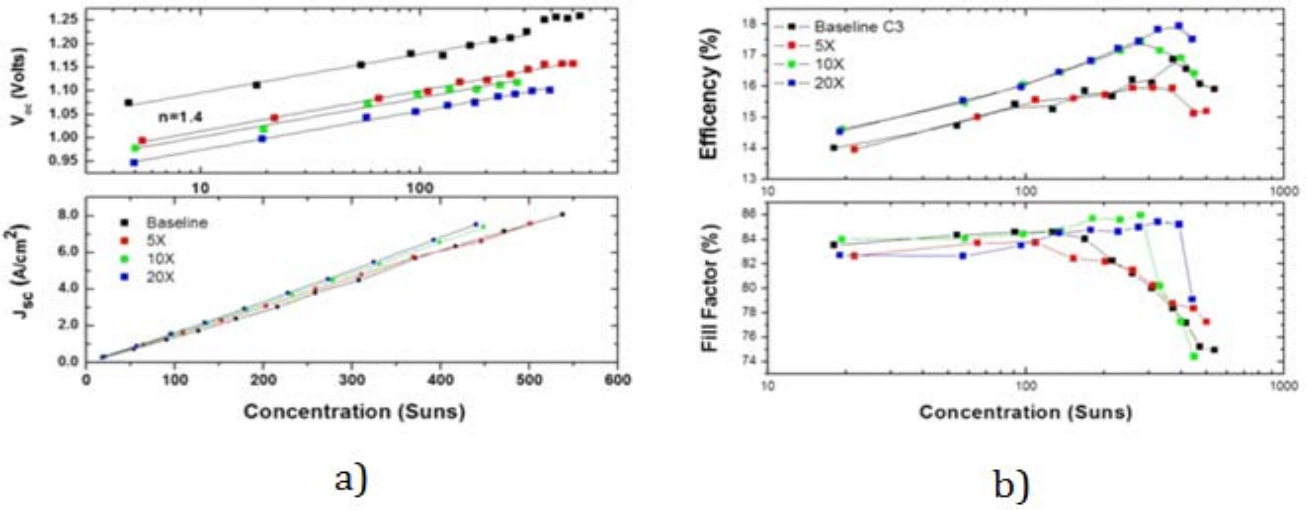

Figure 11. Change in a) V_{OC}, J_{SC}, b) efficiency (16% for no QD, 17% for 10x) and fill factor (84% for no QD, 86% at 10x) with concentration ratio. Solar baseline with no QDs is compared against increased QD concentration. [37]

As quantum dot concentration within the concentrating film increases, photon path length before being emitted into the cell extends as well, lowering the level of fluorescent emission reaching the cell. This places a limiting factor on quantum dot concentration. It can be seen that while concentration ratio could be increased to nearly 600 suns, relative current density and voltage gains are minimal whilst fill factor and efficiency experience substantial losses (Fig. 11).

Monte Carlo modelling and experimental work [39] explored the influences on concentration ratio in LSCs. To prevent non-radiative recombination, the QDs need to have a high absorbance coefficient α_1 for high energy light, but a low absorbance coefficient α_2 for lower-energy light, to prevent reabsorption of emitted low-energy photons. This gives us a quality factor Q_{LSC}, as a ratio of the high-energy absorbance coefficient, to the low energy absorbance coefficient:

$$\mathbf{Q_{LSC}} = \frac{\boldsymbol{\alpha_1}}{\boldsymbol{\alpha_2}} \tag{14}$$

The LSC cells were mirrored on only two sides, and looked at QDs with Q_{LSC} of 1.64, 10.9 and 74.2. [39] Under irradiance from 1-10mW/cm^2 they had a maximum concentration factor of 0.45, 6.5 and 26 respectively. In this system, some loss was due to imperfect transmittance between the LSC unit and the receiving cell, others due to non-radiative recombination, and escape cone losses. Concentration ratio is directly proportional to Q_{LSC} when only two sides of the concentrator are internally reflecting, and to 2 Q_{LSC} in the case when all but one side of the cell are mirrored to fully reflect the emitted frequencies from the quantum dots towards the PV cell. On average, however, concentration increase with increased surface area dropped off after 60cm, as did optical efficiency. Thus it can be seen that the efficiency of

quantum dot solar concentrators have limiting factors both in their quantum collection, quantum yield, and transmittance, with a surface limited optically efficient surface area range.

Benefits of quantum dot concentrators are that they are easily produced and integrated into a solar cell, they have reduced heat production compared to non-concentrated cells, and they are more heat-stable than traditional organic luminescent dyes. [29] Difficulty in producing ideal materials with high Q_{LSC} prevent considerable progress in their implementation as solar concentrators at present time.

3.3.4 Dielectric Totally Internally Reflecting Concentrator

The *dielectric totally internally reflecting concentrator* (DTIRC) is a type of secondary, non-imaging optical concentrator for photovoltaic cells. [40] The device is made from a dielectricum, the refractive index of which allows the device to totally internally reflect and channel light received within an acceptance angle towards a collector. [29,41] DTIRCs can approach the thermodynamic theoretical limit for solar concentration.

The concentrator is comprised of three main components (Fig. 11): a curved front surface (1), a totally internally reflecting profile (2) and an exit aperture (3). The curved front surface can take the form of a hemisphere, parabola or ellipse.

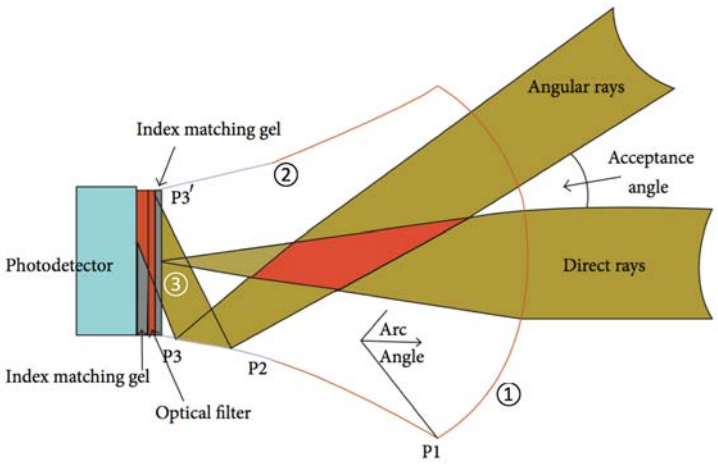

Figure 11. Edge-on schematic of DTIRC design. [22]

When the incident rays from the sun strike the concentrator, they are refracted by the curved front surface and hit the totally internally reflecting profile. If the rays lie within the acceptance angle they are totally internally reflected to the exit aperture. If the rays lie outside the acceptance angle they are reflected away from the side profile and leave the concentrator.

The side profile is comprised of two regions: P1→P2 which is closer to the curved surface, and P2→P3 the remainder of the side profile closer to the exit aperture. Rays that enter the concentrator cell at an angle are reflected off the P1→P2 profile and all strike the single focal point P3'. As for the P2→P3 profile, there are two different fabrication techniques: the maximum concentration method (MCM) and

the phase concentration method (PCM). The MCM is designed to totally internally reflect all rays from P2→P3 to the exit aperture, while the PCM allows all waves to exit in parallel and therefore wavefronts to pass through the exit aperture. This is in direct comparison to compound parabolic concentrators (CPCs), which do not have a side profile that is divided into two different parts. Instead it is simply parabolic; all rays are directed to P3 and P3' in the 2 dimensional schematic. MATLAB simulations to optimize parameters of the DTIRC concluded that the MCM offers a higher gain in concentration on the exit aperture, as it does not restrict the exit or incidence angle. [10] However, this comes at the cost of a larger height and entrance diameter, resulting in a larger concentrator structure.

Compared to CPCs, DTIRCs have higher efficiency, concentration ratio and smaller sizes. Furthermore, cooling systems are not required, reducing the overall bulk of the system. [23] However, the incident light on a DTIRC cannot be efficiently transferred to a cavity of a lower index media, where it can be used in other parts of the cell for power generation. 50% of the light received on the curved surface is reflected off the exit aperture. These various factors limit the overall efficiency of the concentrator. NASA has designed a DTIRC/flux extractor to solve these issues. [24-25] A dielectric rod connects the exit aperture of the DTIRC to the receiving cavity. It allows the extraction of flux from the concentrator cell to the other parts of the solar cell for more efficient use.

Mirror symmetrical dielectric totally internally reflecting concentrators (MSDTIRCs) are a variation of the DTIRC. MSDTIRCs are based on PCM, abandoning rotational symmetry for mirror symmetry about four axes parallel to the concentrator base.

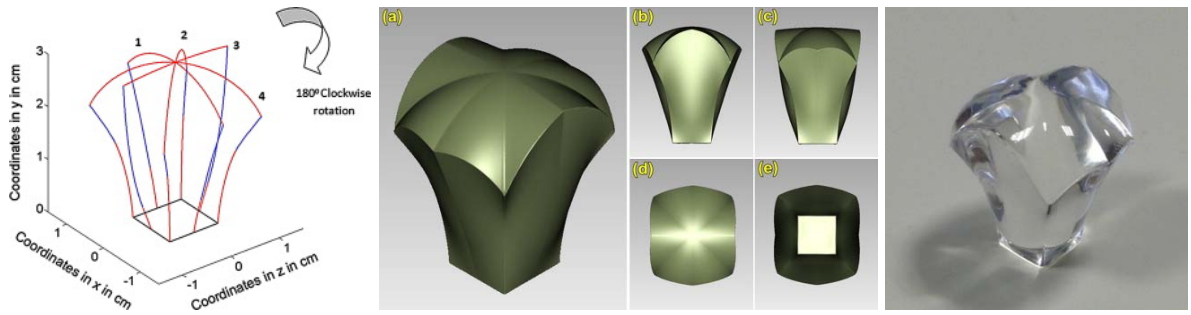

Figure 12. Various MSDTIRC design representations. [26-27]

Experiments conducted under 1kWm^{-2} solar illumination, the MSDTIRC caused the short-circuit current to increase by a factor of 4.2, the maximum power by a factor of 4.6, and the fill factor from 78.5% to 79.7%. Furthermore, when the temperature increased over time, the short-circuit current remained minimal, but the open-circuit voltage fell significantly. By extension, the maximum power and fill factor saw a decreasing trend.

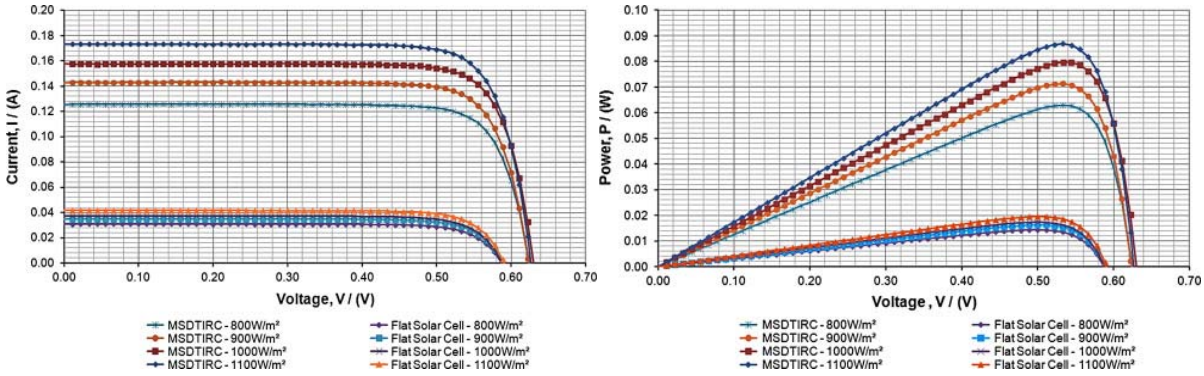

a) b)

Figure 12. a) I-V and b) P-V characteristics for MSDTIRC and flat solar cell configurations under varying solar illumination. [49]

Table 3. Performance of a MSDTIRC system with 5 hours of irradiance at 1kW/m^{-2}. [49]

Time (h)	*Temperature (°C)*	*Maximum power, P_{max} (mW)*	*Maximum current, I_{max} (mA)*	*Maximum voltage, V_{max} (mV)*	*Fill factor, FF*
0.0	25	69	131	526	0.79
0.5	50	62	131	470	0.77
1.0	54	61	131	463	0.76
1.5	56	60	131	460	0.76
2.0	57	60	131	459	0.76
2.5	58	60	131	457	0.76
3.0	58	60	131	455	0.76
3.5	59	60	130	458	0.76
4.0	58	60	131	458	0.76
4.5	58	60	131	459	0.76
5.0	58	60	131	456	0.76

Table 4. Comparison of concentrator designs for SBSP uses

Type	*Concentration Ratio*	*Cell Efficiency Increase*	*J_{SC}*	*V_{OC}*	*FF*	*Optical Efficiency*
Fresnel Lens (CaF_2)	17 200	4.9% 7.5%	1577% 20108%	11.5% 20.6%	4.0% 4.8%	92%
Microlens Array (600μm)	1	3.18%	15.32%	0.93%	0.36%	89%
Quantum Dot (10x Layers)	200-300	0.5%	-	-9%	-	0.1%
DTIRC	4.2	3%	322%	361%	1.2%	-

4. Conclusions

Space based solar power requires a flexible range of design parameters to deal with a wide range of mission requirements. We find that Fresnel Lens concentrators are well suited to space applications as the flat geometry of the Fresnel lens lends itself well to large concentration ratios, whilst still performing exceptionally at lower ratios condusive to temperature sensitive missions. Large aperture lenses can be deployed at an appropriate distance to the cell and vastly increase the intensity of incident sunlight. J_{SC} is shown to scale linearly with concentration, increasing by a factor of 16.8 and 202 at 17 suns and 200 suns, respectively (Tab. 2). The 200 sun case is likely superlinear due to a temperature induced decrease in cell bandgap, allowing more low energy photons to be absorbed.

DTIRC systems are capable of a modest 4.2 sun concentration ratio and 3% boost in efficiency over bare cells (Tab. 4) and fare reasonably well with temperature, seeing a 13.3% drop in V_{OC} with an increase of 33°C (Tab. 3) which is negated by the concentration increase. However, without convective cooling in space the performance can be expected to decrease. The bulk mass required, as well as the additional components necessary to efficiently couple collected light to the cell make it a poor choice for SBSP.

The microlens array shows an appreciable increase in J_{SC} due to the redirection of photons away from front panel contacts, resulting in an equivalent efficiency increase to the DTIRC without adding any appreciable mass or volume to the system. Optical efficiency could likely be improved by replacing the PMMA resin with a more broadband transparent material such as MgF_2 or CaF_2 (Fig. 5). Whilst BK7 boasts exceptional transparency over a broad range the density of borosilicate glasses (Tab. 2) makes it undesirable for large scale implementation in SBSP concentrator lenses.

Quantum dot concentrator designs still lack the engineering necessary to be worthwhile space based concentrators. V_{OC} is seen to decrease due to intrinsic radiative recombination, and J_{SC} shows no significant difference to bare cells.

Concentration ratio should not place the subcell current density in excess of the tunnelling current density of inter-subcell tunnel junctions in order to prevent bottlenecking and efficiency loss. Increased concentration induced temperatures will also be harder to cool with only radiative cooling and heat sinks, resulting in decreased V_{OC}. As typical AlGaAs/GaAs tunnel junctions demonstrate tunnelling currents well above realistic concentration ratios (Fig. 7), temperature will always be the limiting factor. Increasing the tunnel junction bandgap drastically reduces the tunnelling current whilst allowing more sub-bandgap light to pass, and can be an effective strategy for tuning current matching conditions in a cell under concentration.

Acknowledgments

We would like to thank Jurgen Schulte for his guidance in the completion of this project, as well as our fellow students and library staff for their dedicated assistance and feedback.

References

1. Glaser, P. (1968). *Power from the Sun: Its Future.* Science, 162(3856), pp.857-861. doi: http://dx.doi.org/10.1126/science.162.3856.857
2. Ernst, D. (2013). *Beam It Down, Scotty: The Regulatory Framework for Space-Based Solar Power.* Rev Euro Comp & Int Env Law, 22(3), pp.354-365. doi: http://dx.doi.org/10.1111/reel.12041
3. Macauley, M. and Davis, J. (2002). *An economic assessment of space solar power as a source of electricity for space-based activities.* Space Policy, 18(1), pp.45-55. doi: http://dx.doi.org/10.1016/S0265-9646(01)00056-X
4. Carroll, B. and Ostlie, D. (2007). *An introduction to modern astrophysics.* San Francisco: Pearson Addison-Wesley.
5. Markvart, T. (2008). *Solar cell as a heat engine: energy-entropy analysis of photovoltaic conversion.* phys. stat. sol. (a), 205(12), pp.2752-2756. doi: http://dx.doi.org/10.1002/pssa.200880460
6. Würfel, P. (1988). *Generation of entropy by the emission of light.* Journal of Physics and Chemistry of Solids, 49(6), pp.721-723. doi: http://dx.doi.org/10.1016/0022-3697(88)90206-5
7. Ermer, J.H. et al. (2012). *Status of C3MJ+ and C4MJ production concentrator solar cells at spectrolab.* Photovoltaics, IEEE Journal of, 2(2), pp.209-213. doi: http://dx.doi.org/10.1109/JPHOTOV.2011.2180893
8. Www2.pvlighthouse.com.au. (2016). *PVLighthouse - Spectrum library.* [online] Available at: https://www2.pvlighthouse.com.au/resources/optics/spectrum%20library /spectrum%20library.aspx [Accessed 7 May 2016].
9. Algora, C. et al. (2009). *III–V multijunction solar cells for ultra-high concentration photovoltaics.* Photovoltaic Specialists Conference (PVSC), 2009 34th IEEE pp. 1571-1575. doi: http://dx.doi.org/10.1109/PVSC.2009.5411372
10. Cotal, H., et al. (2009). *III–V multijunction solar cells for concentrating photovoltaics.* Energy & Environmental Science, 2(2), pp.174-192. doi: http://dx.doi.org/10.1039/B809257E
11. Luque, A. and Hegedus, S. eds. (2011). *Handbook of photovoltaic science and engineering.* John Wiley & Sons.
12. Rohatgi, A. (2015). *WebPlotDigitalizer* [Online] Available at: http://arohatgi.info/WebPlotDigitizer/ app/ [Accessed on November 2012].
13. Varshni, Y. (1967). *Temperature dependence of the energy gap in semiconductors.* Physica, 34(1), pp.149-154. doi: http://dx.doi.org/10.1016/0031-8914(67)90062-6
14. O'Donnell, K.P. and Chen, X. (1991). Temp*erature dependence of semiconductor band gaps.* Applied Physics Letters, 58(25), pp.2924-2926. doi: http://dx.doi.org/10.1063/1.104723
15. Kinsey, G. et al. (2008). *Concentrator multijunction solar cell characteristics under variable intensity and temperature*. Prog. Photovolt: Res. Appl., 16(6), pp.503-508. doi: http://dx.doi.org/10.1002/pip.834
16. Nishioka, K. et al. (2005). *Evaluation of temperature characteristics of high-efficiency InGaP/InGaAs/Ge triple-junction solar cells under concentration.* Solar Energy Materials and Solar Cells, 85(3), pp.429-436. doi: http://dx.doi.org/10.1016/j.solmat.2004.05.008
17. Nishioka, K et al. (2006). *Evaluation of InGaP/InGaAs/Ge triple-junction solar cell and optimization of solar cell's structure focusing on series resistance for high-efficiency concentrator photovoltaic systems*. Solar Energy Materials and Solar Cells, 90(9), pp.1308-1321. doi: http://dx.doi.org/10.1016/j.solmat.2005.08.003
18. Green, M.A. et al. (2015). *Solar cell efficiency tables (Version 45).* Progress in photovoltaics: research and applications, 23(1), pp.1-9. doi: http://dx.doi.org/10.1002/pip.2573

19. Algora, C. and Rey-Stolle, I. (2016). *Handbook on Concentrator Photovoltaic Technology.* John Wiley & Sons. doi: http://dx.doi.org/10.1002/9781118755655
20. Martí, A. and Luque, A. (2004). *Next generation photovoltaics.* Bristol: Institute of Physics. doi: http://dx.doi.org/10.1887/0750309059
21. King, R. (2002). *High-Efficiency Space and Terrestrial Multijunction Solar Cells Through Bandgap Control in Cell Structures. Photovoltaic Specialists Conference,* 2002. Conference Record of the Twenty-Ninth IEEE, pp.776-781. doi: http://dx.doi.org/10.1109/PVSC.2002.1190685
22. Cotal, H. (2000). *Highly Efficient 32.3% Monolithic GaInP/GaAs/Ge Triple Junction Concentrator Solar Cells.* NCPV Program Review Meeting 2000, pp.111-112.
23. Nishioka, K. et al. (2006). *Evaluation of InGaP/InGaAs/Ge triple-junction solar cell and optimization of solar cell's structure focusing on series resistance for high-efficiency concentrator photovoltaic systems.* Solar Energy Materials and Solar Cells, 90(9), pp.1308-1321. doi: http://dx.doi.org/10.1016/j.solmat.2005.08.003
24. Karam, N. et al. (2001). *Recent developments in high-efficiency Ga0.5In0.5P/GaAs/Ge dual- and triple-junction solar cells: steps to next-generation PV cells*. Solar Energy Materials and Solar Cells, 66(1-4), pp.453-466. doi: http://dx.doi.org/10.1016/S0927-0248(00)00207-5
25. Hermle, M. et al. (2008). *Numerical simulation of tunnel diodes for multi-junction solar cells.* Prog. Photovolt: Res. Appl., 16(5), pp.409-418. doi: http://dx.doi.org/10.1002/pip.824
26. García, I. et al. (2012). *Performance analysis of AlGaAs/GaAs tunnel junctions for ultra-high concentration photovoltaics.* Journal of Physics D: Applied Physics, 45(4), p.045101. doi: http://dx.doi.org/10.1088/0022-3727/45/4/045101
27. Andreev, V. (2006). *Tunnel Diode Revealing Peculiarities at I-V Measurements in Multijunction III-V Solar Cells.* 2006 IEEE 4th World Conference on Photovoltaic Energy Conference, 1, pp.799-802. doi: http://dx.doi.org/10.1109/WCPEC.2006.279577
28. Babar, M. and Al-Ammar, E.A. (2013). *Simulation and Modeling of Multi-junction Solar Cell for Concentrated Photovoltaics using MATLAB/Simulink.* Recent Advances in Energy, Environment and Development, p.36.
29. Khamooshi, M. et al. (2014). *A Review of Solar Photovoltaic Concentrators.* International Journal of Photoenergy, 2014, pp.1-17. doi: http://dx.doi.org/10.1155/2014/958521
30. Fresnel Lenses. (2016). *Thorlabs* [Online] Available at: http://www.thorlabs.hk /newgrouppage9.cfm?objectgroup_id=1222, [Accessed on 15 May 2016]
31. Optical Materials. (2016). *Newport*. [Online] https://www.newport.com/optical-materials, [Accessed on 15 May 2016]
32. Cotal, H. and Sherif, R. (2005). *The effects of chromatic aberration on the performance of GaInP/GaAs/Ge concentrator solar cells from Fresnel optics*, Conference Record of the Thirty-first IEEE Photovoltaic Specialists Conference, 2005. doi: http://dx.doi.org/10.1109/PVSC.2005.1488240
33. O'neill, M.J., Entech, Inc. (2000). *Stretched Fresnel lens solar concentrator for space power*. U.S. Patent 6,075,200.
34. Nam, M. et al. (2013). *Concentrating microlens array mounted on an InGaP/GaAs/Ge solar cell for photovoltaic performance enhancement*, Solar Energy, vol 91, pp.374-380. doi: http://dx.doi.org/10.1016/j.solener.2012.09.011
35. Winston, R. (2011), *Thermodynamics Illuminates Solar Optics*, SPIE Newsroom. doi: http://dx.doi.org/10.1117/2.1201106.003494
36. Chou, K.F. and Dennis, A.M., (2015). *Förster Resonance Energy Transfer between Quantum Dot Donors and Quantum Dot Acceptors*. Sensors, 15(6), pp.13288-13325. doi: http://dx.doi.org/10.3390/s150613288

37. Hubbard, S.M. et al. (2009). *Characterization of quantum dot enhanced solar cells for concentrator photovoltaics.* Photovoltaic Specialists Conference (PVSC), 2009 34th IEEE pp. 90-95. doi: http://dx.doi.org/10.1109/PVSC.2009.5411726
38. Schubert, E.F. et al. (2005). *Light emitting diodes*. John Wiley & Sons, Inc. doi: http://dx.doi.org/10.1016/b0-12-369401-9/00498-8 and http://dx.doi.org/10.1002/0471238961.1209070811091908.a01.pub2
39. Klimov, V. et al. (2016). *Quality Factor of Luminescent Solar Concentrators and Practical Concentration Limits Attainable with Semiconductor Quantum Dots.* ACS Photonics. doi: http://dx.doi.org/10.1021/acsphotonics.6b00307
40. Ning, X. et al. (1987). *Dielectric totally internally reflecting concentrators.* Appl. Opt., 26(2), p.300. doi: http://dx.doi.org/10.1364/AO.26.000300
41. Chaves, J. (2015). *Introduction to nonimaging optics.* CRC Press. doi: http://dx.doi.org/10.1201/b18785
42. Ramirez-Iniguez, R. and Green, R.J. (2005). *Optical antenna design for indoor optical wireless communication systems. International Journal of Communication Systems*, 18(3), pp.229-245. doi: http://dx.doi.org/10.1002/dac.701
43. Muhammad-Sukki, F. et al. (2011). *Optimisation of Concentrator in the Solar Photonic Optoelectronic Transformer: Comparison of Geometrical Performance and Cost of Implementation.* Proceedings of International Conference on Renewable Energies and Power Quality.
44. Muhammad-Sukki, F. et al. (2010). *Solar Concentrators*. International Journal of Applied Sciences, 1(1).
45. Piszczor, M. and Macosko, R. (2000). *A High-Efficiency Refractive Secondary Solar Concentrator for High Temperature Solar Thermal Applications*. Technical Memorandum, NASA.
46. Soules, J. et al. (1997). *Design and Fabrication of a Dielectric Total Internal Reflecting Solar Concentrator and Associated Flux Extractor for Extreme High Temperature (2500K)* Applications. NASA Contractor Report.
47. Muhammad-Sukki, F. et al. (2014). *Mirror symmetrical dielectric totally internally reflecting concentrator for building integrated photovoltaic systems*. Applied Energy, 113, pp.32-40. doi: http://dx.doi.org/10.1016/j.apenergy.2013.07.010
48. Abu-Bakar, S. et al. (2015). *Optimisation of the performance of a novel rotationally asymmetrical optical concentrator design for building integrated photovoltaic system.* Energy, 90, pp.1033-1045. doi: http://dx.doi.org/10.1016/j.energy.2015.07.133
49. Muhammad-Sukki, F. et al. (2013). *Performance analysis of a mirror symmetrical dielectric totally internally reflecting concentrator for building integrated photovoltaic systems.* Applied Energy, 111, pp.288-299. doi: http://dx.doi.org/10.1016/j.apenergy.2013.05.006
50. Nishioka, K. et al. (2006). *Annual output estimation of concentrator photovoltaic systems using high-efficiency InGaP/InGaAs/Ge triple-junction solar cells based on experimental solar cell's characteristics and field-test meteorological data*. Solar Energy Materials and Solar Cells, 90(1), pp.57-67. doi: http://dx.doi.org/10.1016/j.solmat.2005.01.011
51. García, I. et al. (2012). *Performance analysis of AlGaAs/GaAs tunnel junctions for ultra-high concentration photovoltaics*. Journal of Physics D: Applied Physics, 45(4), p.045101. doi: http://dx.doi.org/10.1088/0022-3727/45/4/045101